The Monte Carlo Method: Versatility Unbounded In A Dynamic Computing World
Chattanooga, Tennessee, April 17–21, 2005, on CD-ROM, American Nuclear Society, LaGrange Park, IL (2005)

COMPARISON OF PHANTOM MODELS FOR EXTERNAL DOSIMETRY COMPUTATIONS

Michael W. Mallett and Richard H. Olsher
Los Alamos National Laboratory
HSR-4, MS G761
P.O. Box 1663
Los Alamos, NM 87545
mallett@lanl.gov; dick@lanl.gov

ABSTRACT

Advances in computer processing and Monte Carlo codes have made practical the ability to perform detailed dosimetric computations featuring realistic human models. Both the albedo and radiation attenuation properties of the human model contribute to the accuracy of the computed dose. An assessment of the effect of phantom models on the computed external dose is thus warranted and achievable. The Los Alamos National Laboratory (LANL) uses a thermo-luminescent dosimeter (TLD) capable of measuring both photon and neutron personal dose equivalent, $H_p(d)$. In order to study the impact of the phantom design on the computed dose, a detailed model of the TLD employed at LANL was developed and used to compare phosphor responses for various phantom models. Included in the study were the standard ISO water-filled slab phantom routinely used for calibrations, the MIRD stylistic computational phantom, and the NORMAN tomographic computational phantom. Response of the LANL dosimeter for typical irradiation geometries was calculated using the MCNP and MCNPX codes. The results were compared with computed photon and neutron personal dose equivalents tabulated in ICRP 74. The most significant differences were attributed to perturbation of the albedo neutron signal due to the inclusion of the sternum in the NORMAN phantom.

Key Words: phantom, dosimetry, personal dose equivalent, albedo, angular response

1 INTRODUCTION

Occupational external radiation exposure of personnel at the Los Alamos National Laboratory (LANL) is measured using the custom LANL-design Model 8823 thermoluminescent dosimeter (TLD) [1]. The design of the dosimeter and algorithm permits isolation of the response due to the measured photon, beta, and neutron exposure. Functional corrections determined by the relative elemental responses are used to calculate the personal dose equivalent, $H_p(d)$: for photons, via the relative response of filtered LiF and CaF_2 phosphors; for neutrons, via the relative response of direct and albedo net neutron signals.

A detailed model of the LANL 8823 dosimeter was developed suitable for use with the MCNP/MCNPX codes [2, 3]. This model facilitates evaluation of the dosimeter for a variety of source and geometry conditions, including those too difficult or impossible to achieve in the laboratory (e.g. monoenergetic source energies, no room return). Furthermore, computations performed using the model permit assessing the response of the dosimeter for various occupational environments, in particular those where the measurements would be unfeasible to perform empirically (e.g. extremely low dose rates).

Calibration irradiations in the laboratory are typically performed with the dosimeter mounted on a simple standard phantom (e.g. a solid Lucite* slab). However, the continued evolution in dynamic computer processing, coupled with the expanded capabilities of Monte Carlo codes, affords enhanced opportunities for dosimetric computations. First, more realistic human models can be employed in Monte Carlo computations. This includes stylistic computational models which are described using mathematical shapes and volumes, and tomographic computational models which are generated via CT/MRI images of the human body and consist of millions of voxels of data. Second, a large number of histories can be processed in a reasonable amount of time, thus minimizing a heavy dependence on variance reductions methods characteristic of computations for relatively small tally volumes (i.e. TLD phosphors). Third, a large set of test variables can be reasonably assessed in systematic fashion (e.g. radiation type, energy, angle of irradiation, shielding, etc.).

This study seeks to assess the importance of the phantom model in measuring the personal dose equivalent as determined by the LANL 8823 dosimeter. First, a comparison of three types of phantom models for standard calibration conditions is made, including the standard ISO water-filled slab phantom, the MIRD stylistic computational phantom, and the NORMAN tomographic computational phantom. Second, the effect of the three phantom models is assessed for alternative irradiation angles of incidence, ranging from 0° (antero-posterior, AP, irradiation geometry) to 180° (postero-anterior, PA, irradiation geometry). Third, the study assesses the effectiveness of the LANL 8823 dosimeter and algorithm for approximating the angular response of the operational quantity, $H_p(d)$, and for estimating the radiological protection quantity effective dose, E, as tabulated in ICRP Publication 74 [4].

2 MONTE CARLO MODELS

The LANL 8823, shown in Figure 1, contains two Harshaw-type† TLD cards, featuring eight TL phosphors as given in Table I. Elements 1 (^{7}LiF:Mg, Ti) and 4 (CaF_2:Mn) are heavily filtered with 600 mg cm^{-2} ABS plastic, and are used for determining penetrating photon exposure. First, the incident photon energy is determined via the ratio of these two elements. At relatively high photon energies ($\geq$ 662 keV), calcium fluoride and lithium fluoride phosphors respond identically. As the photon energy decreases, calcium fluoride overresponds relative lithium fluoride, reaching a maximum at 35-40 keV for the LANL 8823 dosimeter design. Photon $H_p(10)$ is then calculated by applying a correction factor determined as a function of the measured effective photon energy to the average signals of elements 1 and 7 (both ^{7}LiF:Mg, Ti).

Neutron exposure is determined using elements 5-8. Phosphors enriched in ^{6}Li (positions 5 and 8) are sensitive to thermal-energy neutron and photon radiation. Whereas phosphors enriched in ^{7}Li (positions 6 and 7) are insensitive to neutron radiation, the net neutron induced signal can be deduced by paired placement of these two phosphor types within the dosimeter. Elements 5 and 6 are completely surrounded by cadmium except for a small anterior window. This pair measures the net thermal neutron radiation directly incident upon the dosimeter (i.e. the *direct* signal). Elements 7 and 8 are completely surrounded by cadmium except for a small posterior window. This pair forms the classic *albedo* detector, measuring the net thermal neutron

*E. I. du Pont de Nemours and Company, 1007 Market Street, Wilmington, DE 19898.

†Thermo Electron Corporation, 81 Wyman Street, P.O. Box 9046, Waltham, MA 02454-9046.

radiation emerging from the body. The ratio of the direct and albedo signals provides a measure of the degree-of-moderation of the neutron field. A correction factor based upon this ratio is used to correct the highly energy-dependent albedo neutron response to yield an estimate of the neutron $H_p(10)$.

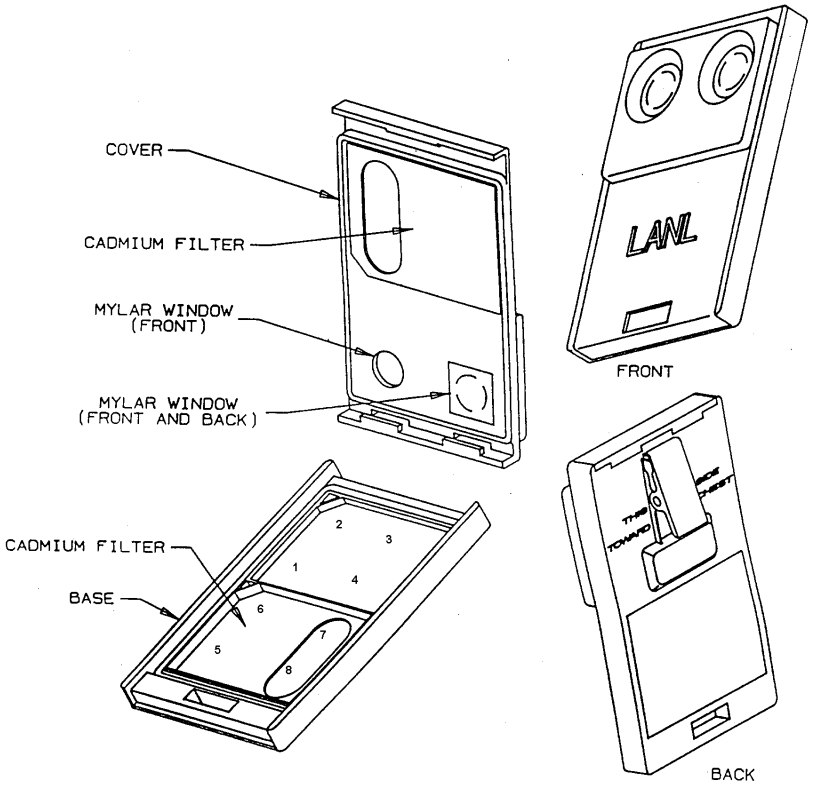

Figure 1. LANL Model 8823 dosimeter cardholder

Table I. LANL Model 8823 dosimeter configuration

Position	TL Phosphor	Filter, Anterior	Filter, Posterior
1	0.38 mm ^{7}LiF:Mg, Ti	ABS, 600 mg cm^{-2}	ABS, 185 mg cm^{-2}
2	0.15 mm ^{7}LiF:Mg, Ti	Mylar, 5 mg cm^{-2}	ABS, 185 mg cm^{-2}
3	0.15 mm ^{7}LiF:Mg, Ti	Mylar, 10 mg cm^{-2}	ABS, 185 mg cm^{-2}
4	0.38 mm CaF_2:Mn	ABS, 600 mg cm^{-2}	ABS, 185 mg cm^{-2}
5	0.38 mm ^{6}LiF:Mg, Ti	ABS, 185 mg cm^{-2}	ABS, 185 mg cm^{-2}, Cd, 460 mg cm^{-2}
6	0.38 mm ^{7}LiF:Mg, Ti	ABS, 185 mg cm^{-2}	ABS, 185 mg cm^{-2}, Cd, 460 mg cm^{-2}
7	0.38 mm ^{7}LiF:Mg, Ti	ABS, 185 mg cm^{-2}, Cd, 460 mg cm^{-2}	ABS, 185 mg cm^{-2}
8	0.38 mm ^{6}LiF:Mg, Ti	ABS, 185 mg cm^{-2}, Cd, 460 mg cm^{-2}	ABS, 185 mg cm^{-2}

The algorithm for the LANL 8823 dosimeter was developed using irradiations that included photon sources with an effective energy ranging from 17 to 662 keV, and bare, polyethylene-, and D_2O-moderated ^{252}Cf fission neutron sources [5]. All irradiations were performed with the dosimeter mounted on a standard 40 cm × 40 cm × 15 cm-thick solid polymethyl methacrylate (PMMA) slab phantom. The elemental responses for each irradiation were used to formulate the correction factors and $H_p(10)$ calculations described above. Whereas the calibration irradiations were performed in less than ideal conditions (e.g. source housing- and room return-induced radiation scattering), the algorithm was redeveloped *in toto* using Monte Carlo computations for direct application to the simulations performed in this study.

2.1 Dosimeter

The Monte Carlo model of the LANL 8823 dosimeter was developed consistent with the input format requirements of the MCNP/MCNPX codes. A cross-sectional view of the TLD Monte Carlo model is shown in Figure 2, illustrating the relative phosphor positions. The dosimeter components were defined using unique cells, surfaces, and materials, created within a separate universe which can easily be added to an existing input file (e.g. detailed occupational environment) via the FILL card. The cell composing the dosimeter universe was 9.1 × cm × 5.5 cm × 1.75 cm-thick. The spaces of this volume not occupied by dosimeter phosphors and miscellaneous holder components were defined as moist air with ρ = 1.2 g cm^{-3}. No S(α,β) treatment was employed for hydrogen bound in the ABS plastic components of the dosimeter holder.

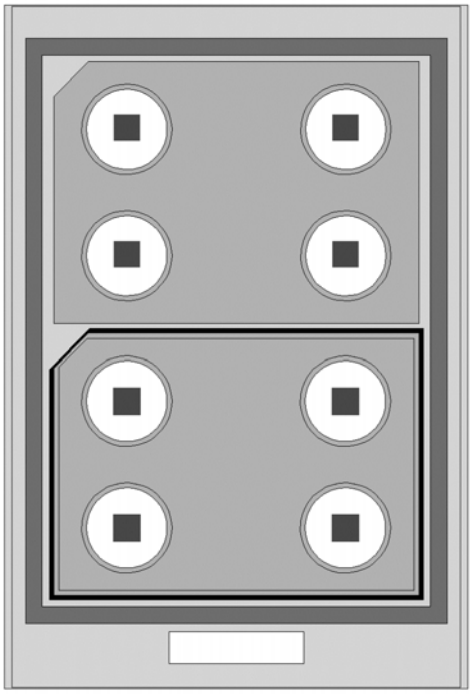

Figure 2. LANL 8823 dosimeter Monte Carlo model

The material compositions of the TL phosphors are given in Table II. Elements 1-4 were mounted on a Kapton substrate (0.06 mm-thick), and elements 5-8 were enclosed between two

layers of Teflon (each 0.05 mm-thick). Tally results were made using the track length estimate of cell heating and energy deposition (F6) in each of the eight phosphor cells.

Table II. TL phosphor material compositions

Material	^{6}LiF:Mg, Ti	^{7}LiF:Mg, Ti	CaF_2:Mn
ρ (g cm^{-3})	2.55	2.65	3.18
^{6}Li (%)[a]	22.47	0.01	–
^{7}Li (%)	1.21	26.42	–
Impurities	Mg, 200 ppm Ti, 10 ppm	Mg, 200 ppm Ti, 10 ppm	Mn, 2.5 %-*m*

[a]Composition by weight.

2.2 Phantom Models

For the Monte Carlo simulations, the dosimeter was centered on the anterior surface of the volume represented by the three phantom models. The vertical position of the dosimeter represented the midpoint of the trunk of the body. The entire length of the phantom was included in the calculations except for the NORMAN phantom. Material definitions for the tissues of the computational phantoms were those previously published by Cristy and Eckerman [6].

2.2.1 ISO Phantom

The standard ISO water-filled slab phantom was modeled as follows [7]:

- External dimensions 30 cm × 30 cm × 15 cm
- Walls constructed of PMMA
- Anterior wall 0.25 cm-thick
- Side and posterior wall 1 cm-thick
- Phantom filled with light water.

S(α,β) treatment for hydrogen bound in light water was made using the lwtr.01t table of the ENDF5 data collection. For hydrogen bound in PMMA, S(α,β) treatment was made using the poly.01t table of the ENDF5 data collection. Monte Carlo simulations performed for a variety of slab phantom constructions (e.g. solid Lucite, polyethylene, and water, etc.) using different S(α,β) treatments for Lucite (e.g., water, no thermal treatment, etc.) validated this approximation.

2.2.2 MIRD Phantom

The MIRD (Medical Internal Radiation Dose) stylistic computational phantom used in the simulations was generated using BodyBuilder, a commercial program from White Rock Science[‡]. The human models produced by BodyBuilder are based on the descriptions for several ages developed by Cristy and Eckerman, and the previous work of Snyder et al. [6, 8-10]. The ORNL models are presented as quadratic and planar equations for the organ surfaces. Specifications are given for the elemental composition of three tissue types: lung, skeletal, and soft tissue. The soft tissue composition is used for all organs other than the skeleton and lungs. All soft tissue organs thus appear the same to a radiation transport simulation. In a few cases, very small changes have been made to organ positions to avoid overlap.

[‡]White Rock Science, P.O. Box 4729, Los Alamos, NM 87544.

BodyBuilder is capable of generating MCNP/MCNPX compatible input files for a phantom of either sex and of arbitrary age, from infant through adult. However, a 21 year old adult male model was used exclusively for all the MIRD-based simulations in this study. Two views of the MIRD phantom model are shown in Figures 3 and 4, including the location of the LANL 8823 dosimeter model on the anterior surface of the phantom.

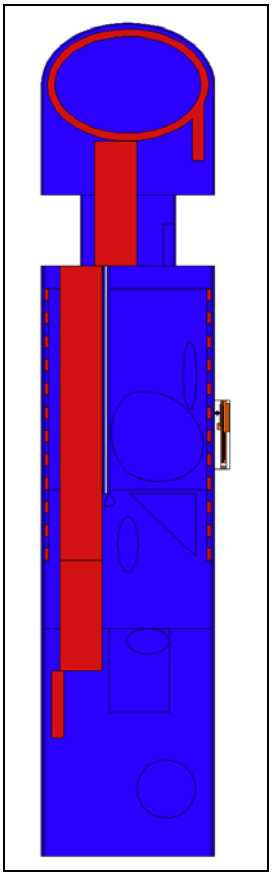

Figure 3. Sagittal view of the MIRD phantom model generated by BodyBuilder, with LANL 8823 dosimeter at anterior surface

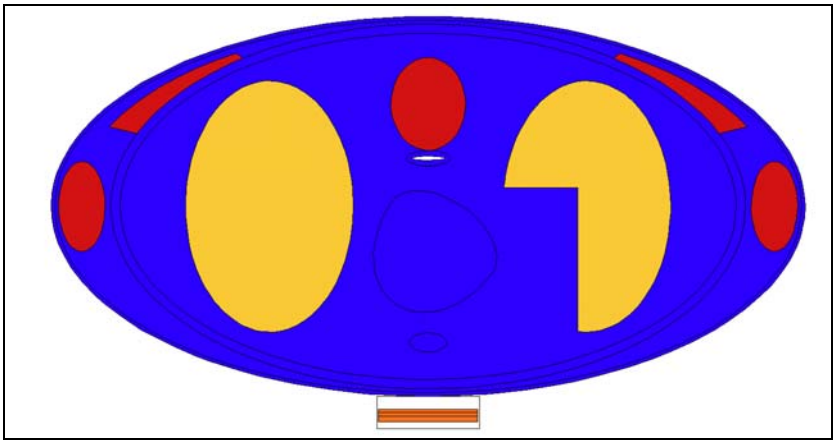

Figure 4. Transverse view of the MIRD phantom model generated by BodyBuilder, with LANL 8823 dosimeter at anterior surface

2.2.3 NORMAN Phantom

The NORMAN tomographic computational phantom was developed by the National Radiological Protection Board (NRPB) using MRI data [11]. The voxels were 2.077 mm × 2.07 mm × 2.02066 mm (vertical length). The block containing the phantom consists of approximately 35 million voxels, about 25% of which form the actual body. Scaling modifications have been made to bring the phantom into close agreement with the size of Standard Man [12]. The vertical size of the voxels was adjusted to make the height of the phantom equal to 1760 mm, and the cross-sectional dimensions were scaled to make the overall weight equal to 73 kg.

Specifications are given for the elemental composition of three tissue types: lung, skeletal, and soft tissue. In addition, air, excluding the lung, and water were defined for the contents of various organs (e.g., esophagus and trachea; bile and stomach contents). The soft tissue composition is used for all organs other than the skeleton and lungs. All soft tissue organs thus appear the same to a radiation transport simulation.

For this study, a subset of the NORMAN database was selected to define a torso phantom model. A total of 226 layers were used, truncating the vertical length to 45.67 cm. This length included the entire lung region, plus an additional 5 cm superior and inferior to the organ. Including further layers made no significant difference in the tally results. The truncated phantom contained more than seven million voxels. Two views of the NORMAN phantom model are shown in Figures 5 and 6, including the location of the LANL 8823 dosimeter model on the anterior surface of the phantom.

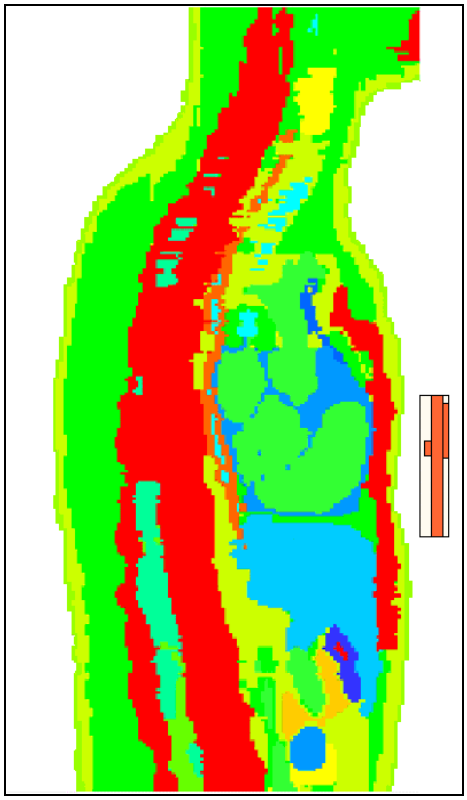

Figure 5. Sagittal view of the NORMAN phantom model, with LANL 8823 dosimeter at anterior surface

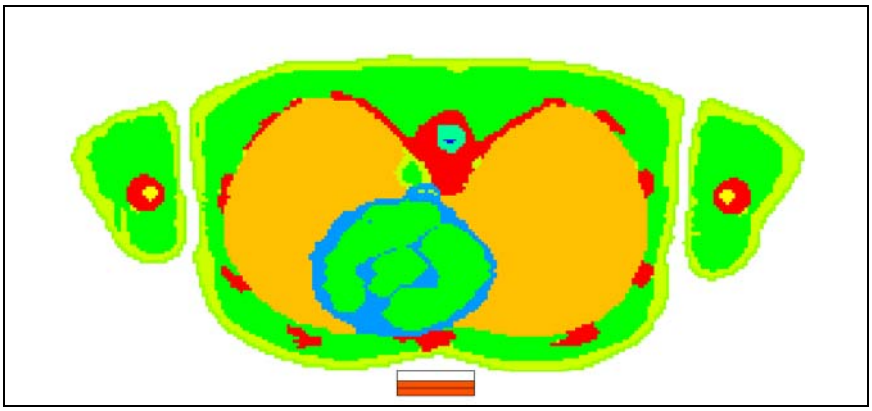

Figure 6. Transverse view of the NORMAN phantom model, with LANL 8823 dosimeter at anterior surface

2.3 Source Specification

All Monte Carlo computations utilized a point source positioned 100 cm from the anterior surface of the phantom for the AP irradiation geometry. The vertical height of the source was consistent with the vertical midpoint of the dosimeter. Photon calculations were performed for monoenergetic sources ranging in energy from 10 keV to 662 keV. Particular emphasis was placed on 20, 36, 70, 120, and 662 keV, as these photon energies represent those historically used for performance testing personnel dosimeters [13]. Also, these energies coincide with unique characteristic features (i.e. local minima and maxima) of the dosimeter algorithm [1].

Neutron calculations were based on ^{252}Cf, the standard neutron source used for performance testing personnel dosimeters [13]. The source was modeled using a Maxwellian fission spectrum with a temperature of 1.42 MeV. A series of computations was also performed with a polyethylene-moderated ^{252}Cf source to simulate the laboratory procedure for calibrating the LANL 8823 dosimeter. In addition to bare ^{252}Cf, the source was surrounded by spherical high-density (ρ = 0.95 g cm^{-3}) polyethylene shells ranging in thickness from 0.6 cm to 15.2 cm, serving to increase the thermal component of the neutron spectrum and decrease the mean neutron energy to about 1.3 MeV (while simultaneously reducing the neutron dose equivalent rate by > 90%).

The effective dose for the various calibration geometries was determined by computing the fluence at the 100 cm distance via the flux at a point (F5) tally. The dosimeter and phantom were not present in these simulations. The calculated fluence was modified by the effective dose per unit fluence data reported in ICRP 74 for the AP irradiation geometry; Tables A.1 and A.17 for photons, and Table A.41 for neutrons.

2.4 General Transport Conditions

In order to assess the isolated effect of the three phantom models upon the response of the LANL 8823 dosimeter, no additional scattering media were included in these simulations. Hence, no room return or in-scattering was present (e.g. from source encapsulation). Likewise, no air was included in the geometry except for that inherent in the phantom definition (e.g. trachea and esophagus organs of the computational phantoms).

Material specifications for photon calculations used the standard photon interaction cross section data based on ENDF/B-IV. Material specifications for neutron calculations used the neutron interaction cross section data ENDF66a and ACTIA libraries of the ENDF/B-VI data collection. No coherent scattering was permitted for photon calculations. Analog capture was exclusively used for neutron calculations. Tally results were generally limited to < 5% relative error, and usually were < 1% relative error. Variance reduction techniques were limited to preferential biasing of the source in the direction of the dosimeter, use of mesh-based weight window generation, and exponential transform for neutron transport. In general, MCNPX 2.5e was used for all MIRD and NORMAN phantom computations, while MCNP5 1.30 was used for all ISO phantom and free-in-air fluence/dose computations.

3 RESULTS AND DISCUSSION

Monte Carlo results are provided below for the LANL 8823 dosimeter calibration and algorithm development, the AP geometry calibration results for each phantom model, the angular dependence results for each phantom model, and the assessment of the dosimeter and algorithm for approximating the angular response of $H_p(d)$ and for estimating E.

3.1 Dosimeter Calibration and Algorithm Development

Development of the LANL 8823 dosimeter algorithm was based upon irradiations using the ISO phantom model. Calibration results for the dosimeter response to photon exposure are given in Figure 7. The ratio of the calcium fluoride-to-lithium fluoride phosphor signals, R41, is shown as a function of the incident photon energy. The value of R41 increases from a normalized value of 1.0 at 662 keV to a maximum of approximately 9.0 at 35-40 keV.

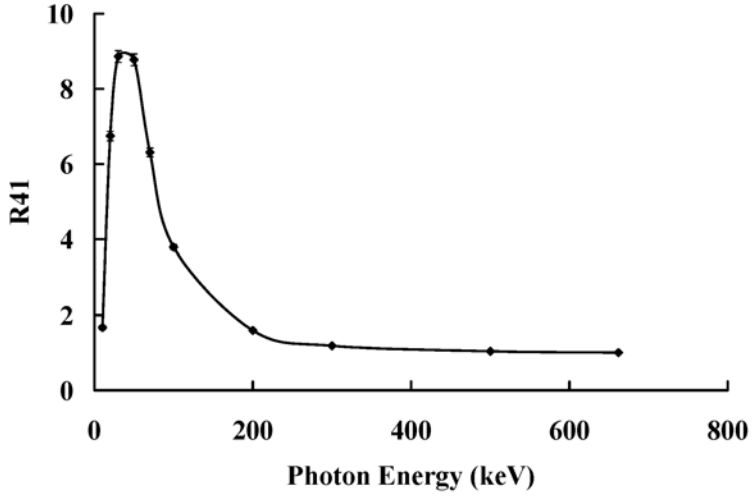

Figure 7. Photon energy discrimination of the LANL 8823 dosimeter, normalized to 662 keV

The dosimeter algorithm uses the data of Figure 7 essentially in reverse. That is, for a given set of eight computed (or measured) elemental responses, R41 is first calculated and the curve of Figure 7 consulted to determine the measured effective photon energy. The algorithm produces

ambiguous results for the measured effective photon energy about the maximum at 35-40 keV. However, exposure to photon energies below 35 keV is characterized by large element 6-to-element 7 ratios (> 5) due to the cadmium filter anterior to element 7.

Figure 8 displays the photon $H_p(10)$ correction factor, normalized to 1.0 at 662 keV, as a function of the incident photon energy. A maximum value of 1.12 is reached at 70 keV, consistent with published values for C_x, the exposure-to-dose equivalent conversion factor for photon calibration of dosimeters mounted on a phantom [5].

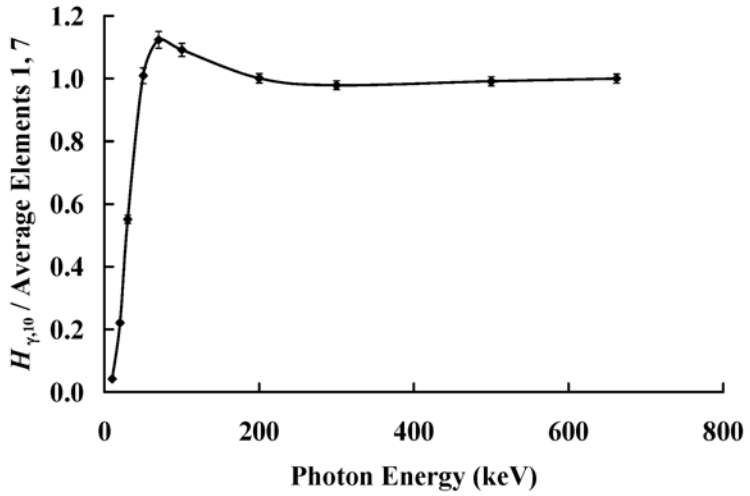

Figure 8. Photon $H_p(10)$ correction factor for the LANL 8823 dosimeter, normalized to 662 keV

The dosimeter algorithm consults the data of Figure 8, based on the measured effective photon energy (Figure 7), to determine the appropriate correction factor for a given set of elemental responses. Photon $H_p(10)$ is then calculated as the multiple of the correction factor and the average responses of elements 1 and 7.

Calibration results for the LANL 8823 dosimeter response to neutron exposure are given in Figure 9. The neutron $H_p(10)$ correction factor is shown as a function of the direct-to-albedo signal ratio, normalized to 1.0 for bare ^{252}Cf. Note that increasing polyethylene moderation of ^{252}Cf yields an increase in the direct-to-albedo signal ratio.

The dosimeter algorithm consults the data of Figure 9, based on the measured direct-to-albedo signal ratio for a given set of elemental responses. Neutron $H_p(10)$ is then calculated as the multiple of the correction factor and the albedo signal response.

The results presented in Figures 7-9 used to regenerate the dosimeter algorithm for calculated data are essentially identical in form to the empirically derived algorithm for the LANL 8823 [1]. The one exception is the continued decrease in the neutron correction factor for an increasing direct-to-albedo signal ratio. In the laboratory, the correction factor reaches a constant minimum for direct-to-albedo signal ratio values above approximately 0.7. This is due to the fact that room return, excluded from these calculations, steadily contributes to the albedo signal for increasing moderation of the ^{252}Cf source.

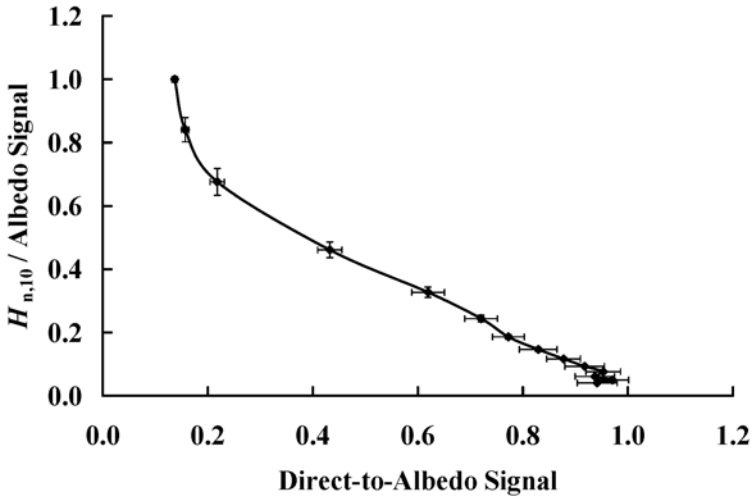

Figure 9. Neutron $H_p(10)$ correction factor for the LANL 8823 dosimeter, normalized to bare ^{252}Cf

3.2 AP Geometry Calibration Results

Monte Carlo calculated $H_p(10)$ results for the AP geometry are reported in Table III. All results are a product of the algorithm as described above. Results are normalized to the calculated response of the LANL 8823 dosimeter for the AP geometry on the ISO phantom.

Table III. AP Geometry $H_p(10)$ Calibration Results[a,b]

		MIRD	NORMAN
Photon:	20 keV	0.983	1.001
	36 keV	0.888	0.905
	70 keV	0.978	0.830
	120 keV	1.002	0.881
	662 keV	1.003	0.952
Neutron:	Bare ^{252}Cf	0.821	1.497

[a]By definition, results for the ISO phantom for all sources equal 1.0.
[b]Using approximate curve fits for the data of Figures 7-9, total uncertainty (1σ) of results is estimated to be < 10%.

Analysis of the AP geometry results is complicated by the inclusion of the sternum in the NORMAN phantom whereas it is absent in the MIRD phantom. This fact means greater density skeleton tissue (ρ = 1.4 g cm^{-3}) is located directly posterior to the LANL 8823 dosimeter for the NORMAN phantom. This structure perturbs the photon backscatter and albedo neutron transport that contributes to the response of the dosimeter. Therefore, additional Monte Carlo computations were performed for the dosimeter repositioned both left and right of center (by 6 cm) on the NORMAN model. The average result for these three dosimeter positions on the NORMAN phantom was 1.159, as compared with the value of 1.497 for the dosimeter located at the median plane reported in Table III.

3.3 Angular Dependence Results

Monte Carlo calculated $H_p(10)$ results for alternative irradiation angles of incidence, 0º to 180º, are reported in Table IV. All results are a product of the algorithm as described above. Results are normalized to the calculated response of the dosimeter for the AP geometry on the ISO phantom. Note that the distance from the source origin to the anterior surface of the phantom model (also the posterior surface of the dosimeter) remained 100 cm for all angles of incidence. Results for the NORMAN phantom are solely for a dosimeter positioned on the median plane.

Table IV. Angular Dependence $H_p(10)$ Results[a]

ISO Phantom

		30º	60º	90º	120º	150º	180º
Photon:	20 keV	1.022	0.636	0.103	0.000	0.000	0.000
	36 keV	1.051	0.927	0.238	0.073	0.088	0.154
	70 keV	0.932	0.779	0.407	0.139	0.227	0.343
	120 keV	0.989	0.824	0.668	0.243	0.275	0.329
	662 keV	0.968	0.957	0.957	0.419	0.407	0.467
Neutron:	Bare ^{252}Cf	0.958	0.662	0.350	0.356	0.505	0.616

MIRD Phantom

		30º	60º	90º	120º	150º	180º
Photon:	20 keV	1.005	0.616	0.153	0.000	0.000	0.000
	36 keV	0.962	0.867	0.306	0.019	0.051	0.015
	70 keV	0.911	0.746	0.442	0.086	0.203	0.173
	120 keV	0.993	0.834	0.722	0.170	0.258	0.223
	662 keV	0.971	0.955	0.978	0.337	0.426	0.341
Neutron:	Bare ^{252}Cf	0.806	0.718	0.335	0.238	0.378	0.374

NORMAN Phantom

		30º	60º	90º	120º	150º	180º
Photon:	20 keV	1.029	0.619	0.109	0.000	0.000	0.000
	36 keV	0.989	0.882	0.420	0.025	0.120	0.035
	70 keV	0.893	0.760	0.470	0.085	0.178	0.210
	120 keV	0.955	0.814	0.665	0.157	0.330	0.246
	662 keV	0.967	0.959	0.942	0.333	0.536	0.349
Neutron:	Bare ^{252}Cf	1.434	1.160	0.622	0.418	0.733	0.846

[a]Using approximate curve fits for the data of Figures 7-9, total uncertainty (1σ) of results is estimated to be < 10%.

The results given in Table IV are in excellent agreement with previously reported empirical results for the LANL 8823 dosimeter [14]. However, this comparison is limited by the fact that the prior study consisted of irradiations restricted to ±85º. In addition, although the neutron exposures were conducted in a low scatter facility, the empirical results included a small contribution from room return.

3.4 Assessment of the Dosimeter and Algorithm for $H_p(10,\alpha)$ and E

Monte Carlo calculated $H_p(10)$ results are shown in Figure 10 for 662 keV photons, and in Figure 11 for bare ^{252}Cf, respectively. Also displayed are ICRP 74 tabulated angular dependence factors for: $H_{p,slab}(10,\alpha)$, computed for the ICRU slab phantom; and for E, computed for various geometries on an adult anthropomorphic computational model. Photon values for $H_{p,slab}(10,\alpha)$ and for E were linearly interpolated at 662 keV from the published data of Table A.24, and Tables A.1 and A.17, respectively. Neutron values for $H_{p,slab}(10,\alpha)$ and for E were derived for a ^{252}Cf Maxwellian fission spectrum (T = 1.42 MeV) from the published data of Tables A.42 and A.41, respectively.

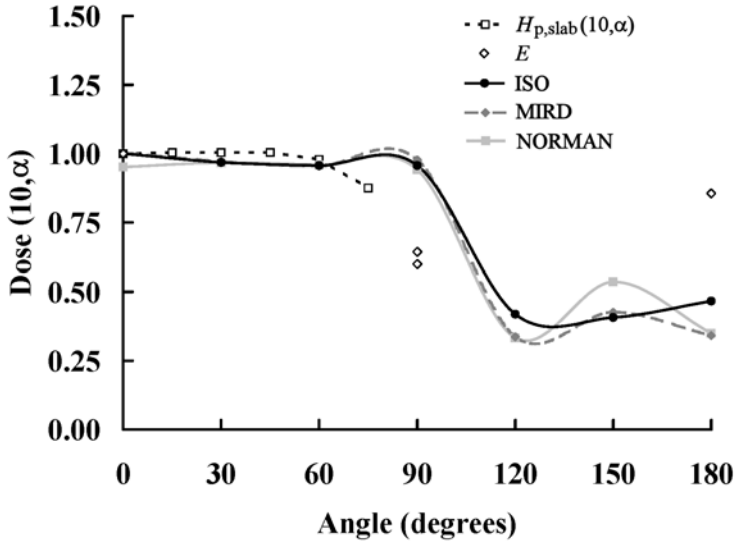

Figure 10. Calculated angular response of the LANL 8823 dosimeter and algorithm for 662 keV photons. LLAT and RLAT values for E are both shown at 90º, (LLAT > RLAT)

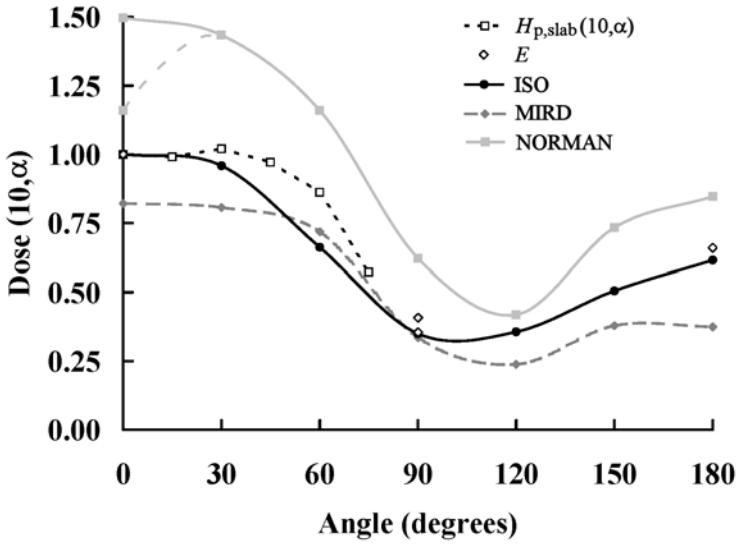

Figure 11. Calculated angular response of the LANL 8823 dosimeter and algorithm for bare ^{252}Cf. LLAT and RLAT values for E are both shown at 90º, (LLAT > RLAT). NORMAN result for average of three anterior dosimeter positions also shown at 0º.

Left lateral (LLAT, 90º) and right lateral (RLAT, 270º) irradiation geometry values reported for E are both shown at 90º, (note LLAT > RLAT). Both values should be considered when reviewing the ISO phantom and MIRD phantom results, as these two models are symmetric about the median plane (except for small differences in the left and right lungs of the MIRD phantom).

Plots are not reproduced here for the additional photon data given in Tables III and IV (i.e. 20, 36, 70, and 120 keV). However, these data were similar in form to that shown in Figure 10. Specifically, the calculated values of $H_p(10)$ for the three phantom models exhibited good agreement with $H_{p,slab}(10,\alpha)$ below 90º, significantly exceeded E and the extrapolated response of $H_{p,slab}(10,\alpha)$ at 90º, and were approximately half the value of the angular dependence factors for E at 180º.

Neutron $H_p(10)$ results for the NORMAN phantom exhibit significant overresponse relative the ISO phantom. This behavior was an artifact of the perturbation of the albedo neutron transport due to the inclusion of the sternum in this model. The effect was a substantial increase in the net neutron albedo signal. Figure 11 also shows the average calculated response for three dosimeter positions, including left and right of center (lateral of the sternum), for the NORMAN phantom at 0º.

This finding calls into question the suitability of using the ISO phantom for neutron calibration irradiations in the laboratory given the more realistic structure of the NORMAN model. In general, it can be observed that LANL personnel do not highly restrict the location of the 8823 dosimeter when donned in the field. For example, the dosimeter is often attached to a shirt collar or labcoat pocket. Likewise, it is often clipped to a lanyard worn about the neck, thereby suspending the dosimeter inferior to the xiphoid process. These observations suggest a non-repeatable geometry not highly susceptible to localized perturbation of the albedo neutron signal by the sternum. Thus, in general, the ISO phantom serves as an acceptable human surrogate when performing neutron calibration irradiations at LANL.

The neutron $H_p(10)$ results for the MIRD phantom exhibit significant underresponse relative the ISO phantom, particularly for those angles closest to the AP and PA irradiation geometries (i.e. < 60 º, and >120º, respectively). This finding is attributed to the oversimplification of the MIRD model, specifically, the large regular-shaped volumes representing the lungs. The impact of these approximations, as evidence by the results of Figure 11, precludes the use of the MIRD phantom as an acceptable human surrogate for neutron calibration irradiations.

4 CONCLUSIONS

For photon exposure, this study shows little difference between the three phantom models. Hence, the ISO phantom serves as an acceptable human surrogate when performing photon calibration irradiations in the laboratory. However, use of the LANL 8823 dosimeter and algorithm may underestimate the effective dose for the unique condition of an expanded and aligned photon field with a large angle of incidence (i.e. greater than approximately 120º).

For neutron exposure, this study shows significant differences for the NORMAN phantom when the dosimeter is located directly anterior to the sternum. However, for the condition when the position of the dosimeter is not highly restricted near the sternum when donned in the field, the ISO phantom serves as an acceptable human surrogate for neutron calibration irradiations in

the laboratory. The study also indicates that the LANL 8823 dosimeter and algorithm well approximate the angular response of $H_p(10)$ and estimate E.

Future work must include the consideration of more realistic irradiation conditions, particularly for neutron computations. This necessarily includes revising the calculated dosimeter algorithm based upon simulations that factor in neutron scattering and room return.

5 REFERENCES

1. J. M. Hoffman, M. W. Mallett, "The LANL Model 8823 Whole-Body TLD and Associated Dose Algorithm," *Operational Radiation Safety, Health Physics Journal (suppl.)*, **Vol. 77 (5)**, pp.S96-S103 (1999).
2. MCNP Monte Carlo Team, X-5, *MCNP5_RSICC_1.30, LA-UR-04-5921*, Los Alamos National Laboratory, Los Alamos, NM (2004).
3. J. S. Hendricks, G. W. McKinney, L. S. Waters, et al., *MCNPX, Version 2.5.e, LA-UR-04-0569*, Los Alamos National Laboratory, Los Alamos, NM (2004).
4. International Commission on Radiological Protection, *Conversion Coefficients for Use in Radiological Protection Against External Radiation, ICRP Publication 74*, Pergamon, Oxford, UK (1996).
5. U.S. Department of Energy, *Department of Energy Standard for the Performance Testing of Personnel Dosimetry Systems, DOE/EH-0027*, U.S. Department of Energy, Washington, D.C. (1986).
6. M. Cristy, K. F. Eckerman, *Specific Absorbed Fractions of Energy at Various Ages from Internal Photon Sources. I. Methods, ORNL/TM-8381/V1*, Oak Ridge National Laboratory, Oak Ridge, TN (1987).
7. International Organization for Standardization, *Reference neutron radiations -- Part 3: Calibration of area and personal dosimeters and determination of response as a function of energy and angle of incidence, ISO 8529-3:1998*, International Organization for Standardization, Geneva, Switzerland (1998).
8. M. Cristy, *Mathematical Phantoms Representing Children of Various Ages for Use in Estimates of Internal Dose, NUREG/CR-1159*, U. S. Nuclear Regulatory Commission, Washington, D.C. (1980).
9. W. S. Snyder, M. R. Ford, G. G. Warner, S. B. Watson, *A Tabulation of Dose Equivalent per Microcurie-day for Source and Target Organs of an Adult for Various Radionuclides: Part I, ORNL-5000*, Oak Ridge National Laboratory, Oak Ridge, TN (1974).
10. K. F. Eckerman, M. Cristy, J. C. Ryman, "The ORNL Mathematical Phantom Series," http://homer.hsr.ornl.gov/VLab/mird2.pdf (1996).
11. D. G. Jones, "A Realistic Anthropomorphic Phantom for Calculating Organ Doses Arising from External Photon Irradiation," *Radiation Protection Dosimetry*, **Vol. 72 (1)**, pp.21–29 (1997).
12. International Commission on Radiological Protection, *Report of Committee II on Permissible Dose for Internal Radiation, ICRP Publication 2*, Pergamon Press, New York, USA (1959).

13. American National Standards Institute, *Personnel Dosimetry Performance – Criteria for Testing, HPS N13.11-1993*, Health Physics Society, McLean, VA (1993).

14. M. W. Mallett, *LANL Model 8823 Personnel Dosimeter Lower Limit of Detectability and Angular Dependence Studies, ESH-4-MTS-97:047*, Los Alamos National Laboratory, Los Alamos, NM (1997).